Very large amplitude intermolecular vibrations and wave function delocalization in 2,3-dimethylnaphthaleneHe van der Waals complex

Andreas Bach, Samuel Leutwyler, Dubravko Sabo, and Zlatko Bačić

Citation: The Journal of Chemical Physics **107**, 8781 (1997); doi: 10.1063/1.475170
View online: http://dx.doi.org/10.1063/1.475170
View Table of Contents: http://scitation.aip.org/content/aip/journal/jcp/107/21?ver=pdfcov
Published by the AIP Publishing

Very large amplitude intermolecular vibrations and wave function delocalization in 2,3-dimethylnaphthalene·He van der Waals complex

Andreas Bach and Samuel Leutwyler
Departement für Chemie und Biochemie, Universität Bern, Freiestrasse 3, CH-3000 Bern 9, Switzerland

Dubravko Sabo and Zlatko Bačić
Department of Chemistry, New York University, 100 Washington Square East, New York, New York 10003

(Received 16 May 1997; accepted 26 August 1997)

We report a combined experimental and theoretical study of the intermolecular vibrations and van der Waals isomerism of the 2,3-dimethylnaphthalene·He van der Waals complex. Two-color resonant two-photon ionization spectra of the $S_0 \rightarrow S_1$ electronic transition of 2,3-dimethylnaphthalene·He exhibit five bands within $30\ \mathrm{cm}^{-1}$ of the electronic origin. The intermolecular potential energy surface was modeled as a sum of atom–atom Lennard-Jones pair potentials; it exhibits two equivalent global minima on each side of the naphthalene moiety, and a single shallower local minimum adjacent to the two methyl groups. Based on this surface, accurate three-dimensional quantum calculations of the van der Waals vibrational levels using the discrete variable representation method were performed. Careful optimization of the potential parameters lead to a quantitative reproduction of four observed bands as intermolecular vibrational excitations, a vibrationally averaged He atom distance from the aromatic plane $\langle z_0 \rangle = 3.22$ Å, and a dissociation energy $D_0(S_1) = -60.3\ \mathrm{cm}^{-1}$, compatible with experiments. The fifth band is assigned as a van der Waals isomer, corresponding to the local minimum. The quantum calculations were extended up to the dissociation limit, yielding ≈ 173 van der Waals vibrational states. Above 70% of D_0, many vibrational states are completely delocalized over the potential surface, with root-mean-square vibrational amplitudes up to 6 Å parallel to and up to 1.5 Å perpendicular to the molecular surface. Calculated tunnelling splittings range from $<10^{-4}\ \mathrm{cm}^{-1}$ for localized states, to $>3\ \mathrm{cm}^{-1}$ for highly delocalized ones. © *1997 American Institute of Physics.* [S0021-9606(97)01745-5]

I. INTRODUCTION

van der Waals (vdW) complexes between an aromatic molecule (M) and one or more helium atoms have been employed as model systems for studying a variety of phenomena at the microscopic level, such as photophysical and photochemical relaxation dynamics, intra/intermolecular vibrational redistribution, vibrational predissociation, physisorption interactions, and nano-solvation.[1–17] For a quantitative description of these and other spectroscopic and dynamical aspects of $M \cdot He_n$ vdW complexes and clusters, accurate three-dimensional (3D) intermolecular potential energy surfaces (IPESs) between M and He are necessary.

Spectroscopy of M·R complexes (R=rare gas atom) has become the main source of information for constructing reliable multidimensional M-R IPESs. Rotationally resolved spectroscopic techniques[1–3,16–24] have determined the equilibrium geometry, i.e., the location of the minimum of the IPES. Excited intermolecular vibrations, which probe regions of the IPES farther away from the minimum-energy region, have been studied using vibrationally resolved spectroscopies in conjunction with quantum methods for calculating accurate 3D vdW vibrational states of M·R complexes, such as vdW complexes of Ar with 2,3-dimethylnaphthalene (2,3-DMN),[25] *o*-xylene,[26] 1,2-DMN,[27] aniline,[28] benzene,[29–31] and Ne with 2,3-DMN.[32]

In contrast to M·Ar complexes, whose excited vdW vibrational level structure has been characterized rather well for a number of aromatics, experimental information on M·He complexes is still relatively scarce. In several of the pioneering laser-induced fluorescence studies in molecular beams, the groups of Levy and later of Smalley investigated the geometric structure and bond lengths of *s*-tetrazine·$He_{1,2}$[1,3,6] and benzene·$He_{1,2}$[2] by high-resolution laser spectroscopy in the visible or UV. The vibronic spectra of the aniline·He[9,12,33] and stilbene·He[4,10,13,14] vdW complexes have been studied by both LIF and resonant two-photon ionization. Vibrational predissociation has also been induced in stilbene·He and proved to be mode-selective.[11,15,16] However, the M-He vdW bond lengths are known only to within ±0.1 Å, and only a single intermolecular excited M-He vibration has so far been observed, for aniline·He.[9] Mostly due to this lack of experimental constraints, little is still known about the IPESs of M·He complexes.

In this work we present a combined spectroscopic and theoretical study of the intermolecular vibrations of the vdW complex 2,3-DMN·He in the S_1 excited electronic state. Compared to other aromatic molecules studied so far, this system exhibits a larger number of intermolecular vibrational excitations, providing stringent constraints on the lower $\approx 40\%$ of the IPES. Interpretation and assignment of the vibronic spectrum rely on the accurate quantum 3D calculations of the intermolecular vibrational $(J=0)$ states of 2,3-DMN·He, using the discrete variable representation (DVR) based method for atom-large molecule complexes developed by Mandziuk and Bačić.[34] As in our previous work on Ne and Ar complexes, the IPES for the S_1 state of 2,3-DMN·He

is represented as a sum of atom–atom Lennard-Jones pair potentials, whose parameters were varied until excellent agreement was achieved between calculated and measured vdW vibrational frequencies.

Helium vdW complexes show extreme quantum mechanical behavior, due to their low binding energies, the small mass of He, and the resulting large vibrational amplitudes. This forced us to extend our 3D DVR calculations to the highest possible accuracy, and to include states up to the dissociation limit in order to obtain numerically converged results and gain insight into the complex quantum dynamics of this system. The very large amplitude of the intermolecular vibrations leads to delocalization of the He wave function around the whole aromatic molecule at very low energy, giving rise to large calculated tunneling splittings.

The intermolecular vibrations and dissociation energies of vdW complexes of toluene, d_8-toluene, *o*-, *m*-, and *p*-xylene, and of 1,2- and 1,8-dimethylnaphthalene with He are described in a following paper.[35] The potential parameters derived in this work for 2,3-dimethylnaphthalene are being tested on these related aromatic systems, and so far reproduce quite accurately the observed intermolecular vibrational frequencies and dissociation energies.[36] We expect the IPES and parametrization developed in this work to be transferable to other aromatic molecules.

The experimental technique and spectroscopic results are discussed in Sec. II. The 3D DVR method for calculating large-amplitude-motion vdW states of 2,3-DMN·He and the computational aspects of the calculations are given in Sec. III. In Sec. IV we compare the experimental and theoretical results, describe the resulting IPES, and discuss the quantum dynamics of highly excited vdW vibrational states of 2,3-DMN·He. The results for 2,3-DMN·R with R=He, Ne,[32] and Ar[25] are compared in Sec. V. Section VI presents the conclusions.

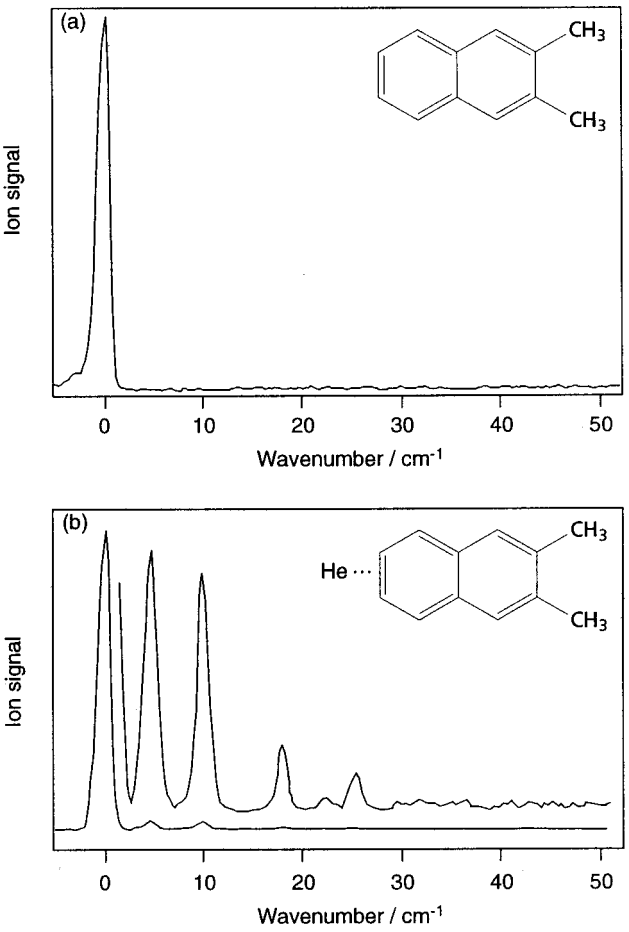

FIG. 1. (a) 2C-R2PI $S_0 \rightarrow S_1$ spectrum of 2,3-DMN, in the vicinity of the electronic origin. Wavenumber scale relative to the 0_0^0 band at 31675.8 cm^{-1}. (b) 2C-R2PI spectrum of 2,3-DMN·He. The origin is blue-shifted by $+2.8$ cm^{-1} relative to bare 2,3-DMN. Intermolecular vdW vibrations (see text) are observed at $+10.3$, $+18.4$, $+22,7$, $+25.9$ cm^{-1}, while the band at $+5.0$ cm^{-1} is due to a second isomer of 2,3-DMN·He.

II. EXPERIMENTAL RESULTS AND DISCUSSION

The 2,3-DMN·He complex was synthesized and cooled in pulsed supersonic expansions of pure helium. Two-color-R2PI spectra were measured using the outputs of two independently tunable frequency-doubled dye lasers which were pumped by the second harmonic of a Nd:YAG laser. Time-of-flight mass spectra were acquired in a 1.0 m linear time-of-flight mass spectrometer. The ion signals were detected on Galileo FTD2003 double-channel plates, digitized in a Sony/Textronix 500 MHz 10-bit transient digitizer, and averaged over 128 laser shots. The experimental setup is described in detail in a companion paper.[35]

The R2PI spectra of the supersonically cooled 2,3-DMN molecule and 2,3-DMN·He vdW complex are shown in Figs. 1(a) and 1(b), respectively. For bare, 2,3-DMN, no bands are observable above the 0_0^0 transition up to a double methyl rotor transition at 163 cm^{-1}.[25,37] The origin of the 2,3-DMN·He vdW complex is blue-shifted by $+2.8$ cm^{-1} relative to that of bare 2,3-DMN. This can be compared to the 2,3-DMN·Ne complex, where the analogous spectral shifts is also to the blue, but only $+1.5$ cm^{-1}, and to the complex with Ar, where the shift is to the red, -4.3 cm^{-1}. In the spectrum of 2,3-DMN·He five additional bands are clearly observed at 5.0, 10.3, 18.4, 22.7, and 25.9 cm^{-1}. These bands are not observed in the pure 2,3-DMN spectrum, and must be due to vdW vibrational excitations and/or isomers. The frequency of the highest observed intermolecular vibration at 25.9 cm^{-1} and the missing intramolecular (methyl rotor) level at 163 cm^{-1} bracket the vdW dissociation energy D_0 in the S_1 state as $25.9 < D_0 < 163$ cm^{-1}. This value is compatible with measured values for other dimethylnaphthalenes, such as 1,8-DMN·He and 1,2-DMN·He, see the discussion in Ref. 35.

III. THEORY AND COMPUTATIONAL ASPECTS

A. The atom–large molecule Hamiltonian and the 3D DVR

The computational method employed in the calculations of 3D intermolecular vibrational ($J=0$) levels of S_1 state 2,3-DMN·He was developed by Mandziuk and Bačić,[34] and applied successfully to a variety of M·R vdW

complexes[25–27,32,34] and the endohedral fullerene complex Ne@C70.[38] In view of these extensive applications and availability of a detailed description,[34] only the key features of this quantum 3D bound state method are summarized here.

Following Brocks and van Koeven,[39] the intermolecular vibrations of such M·R complexes, whose IPESs are highly anisotropic, are treated in terms of three Cartesian components (x,y,z) of the vector connecting the center of mass of the M and the atom R. These are aligned with the principal axes of M, with x and y along the long and short in-plane axes of 2,3-DMN, respectively, and z perpendicular to the naphthalene molecular plane. Brocks and van Koeven have derived the vdW vibrational Hamiltonian in these M-fixed coordinates.[39]

All three intermolecular degrees of freedom are treated in the discrete variable representation (DVR).[40,41] Multidimensional DVRs offer numerous important advantages which are well documented.[32,34,40,41] The grid-like basis in several dimensions can be automatically tailored to the features of the PES and confined to the regions of the potential which are accessible at the excitation energies of interest. It also eliminates the need for numerical integration when evaluating potential matrix elements, which simplifies and speeds up the calculations. DVR of two or more internal degrees of freedom allows particularly effective implementation of the successive diagonalization and truncation procedure devised by Bačić and Light.[40–43] This technique generates a compact quasiadiabatic vibrational basis which reduces drastically the size of the final Hamiltonian matrix, while preserving the accuracy of the calculated eigenstates.

B. Symmetry-adapted 3D DVR and computational parameters

As in our previous calculations of M·R complexes, the 3D DVR is constructed as a direct product of 1D DVRs defined by 1D harmonic oscillator (HO) functions in x, y, and z, respectively, centered in the center of mass of 2,3-DMN.[25,32,34] In this work, an alternative 3D DVR was also investigated, consisting of a direct product of 1D DVRs defined by sine functions[44] in x, y, and z, respectively, centered at 2,3-DMN center of mass. The comparative efficiency of the sine vs. the HO basis was extensively tested, and the two were found to be closely comparable in terms of computer time, for the same numerical accuracy.

As for the 2,3-DMN·Ar and 2,3-DMN·Ne complexes studied by us previously,[25,32] the permutation-inversion (PI) symmetry group of 2,3-DMN·He is C_{2v}, when the internal rotation of the methyl groups is not considered. Symmetry adaptation of the 3D DVR to each of the irreducible representations (IRs) of this group is accomplished by employing the appropriate parity for the 1D DVRs: even- and odd-parity 1D DVRs are formed for the y and z coordinates. The 1D DVR in x has no parity and is left unsymmetrized.[34,25,32]

In order to obtain vibrational eigenvalues which are numerically converged to $<0.001\ \mathrm{cm}^{-1}$, extremely large basis sets had to be employed for this vdW complex. The reasons for this are as follows:

(i) Due to its light mass, the He atom attains large vibrational amplitudes, ranging up to 6 Å for high-lying vibrational states.

(ii) Due to the low-lying potential energy barriers, the He atom delocalizes completely around the aromatic molecule, even at low energies. Already for the lowest vibrational levels, large grids of $12\times12\times12\ \text{Å}^3$ had to be employed, and for states $>40\ \mathrm{cm}^{-1}$ these had to be extended to $24\times18\times18\ \text{Å}^3$.

(iii) In addition to its large spatial extent, the intermolecular PES exhibits steep gradients and rapid spatial modulation especially in the repulsive regions close to the aromatic molecule and in the vicinity of the methyl groups, necessitating a very high density of grid points.

The 3D DVR grid used in the final calculations was as follows. Along the x axis, a 1D DVR of $N_x=100$ was used, extending from -12.0 to $+12.0$ Å. The 1D DVR in the y direction had dimension $N_y=50$, and the range $0<y<9.0$ Å. In the z dimension, we employed a 1D DVR of the size $N_z=100$ extending from 0 to 9 Å. Out of the 100 1D (z mode) eigenstates, only the $n_{\mathrm{cut}}^{\mathrm{1D}}=10$ lowest-energy 1D eigenstates for each (x_α, y_β) were retained for the next step. For the last step, $n_{\mathrm{cut}}^{\mathrm{2D}}=35$ lowest-energy 2D (yz) eigenstates, out of 500, were kept at each DVR point x_α along the x axis. The dimension of the final Hamiltonian matrix, diagonalization of which yields the 3D vdW vibrational eigenstates, was $N_x\times n_{\mathrm{cut}}^{\mathrm{2D}}=100\times35=3500$. This is significantly smaller than $N_x\times N_y\times N_z=500\,000$, the size of the primitive, uncontracted 3D DVR basis.

The convergence behavior of the vibrational eigenvalues with increasing basis set size was extensively studied: the starting basis set was $N_x\times N_y\times N_z=40\times40\times40$ functions, equivalent to $N=6.4\times10^4$ functions. With this medium-sized basis, states at $20\ \mathrm{cm}^{-1}$ were only converged to $\approx0.5\ \mathrm{cm}^{-1}$. Increasing the primitive basis to $N_x\times N_y\times N_z=100\times50\times100=5\times10^5$ improved the convergence of states at $40\ \mathrm{cm}^{-1}$ to below $0.001\ \mathrm{cm}^{-1}$, and of states at $\approx60\ \mathrm{cm}^{-1}$, close to the dissociation limit, to below $0.1\ \mathrm{cm}^{-1}$. Due to memory limits, this was the largest calculation which could be performed (400 h on an RS-6000/590 CPU with 1 GB memory).

IV. INTERMOLECULAR VIBRATIONAL STATES OF 2,3-DMN·He

A. Parametrization and potential energy surface

Several different Lennard-Jones (LJ) parametrizations have been proposed by Lim[45,46] for modeling the collisional deactivation of aromatic molecules by helium and other rare gas atoms. We started from his parametrization denoted $tHe-3$,[45,46] with values $\sigma(\text{He–C})=3.099$ Å, $\sigma(\text{He–H})=2.903$ Å, $\epsilon(\text{He–C})=13.92\ \mathrm{cm}^{-1}$ and $\epsilon(\text{He–H})=5.761\ \mathrm{cm}^{-1}$. These LJ parameters were optimized extensively to fit the five experimental bands: the collision parameters σ were individually varied from 2.53 to 3.35 Å in steps

TABLE I. Lennard-Jones parameter set *tHe*3, I and II for 2,3-DMN·He in the S_1 state. σ in Å and ϵ in cm^{-1}.

Parameter	*tHe*3[a]	Set I	Set II
σ(He–C)	3.099	3.100	3.100
σ(He–H)	2.903	2.660	2.660
ϵ(He–C)	13.92	15.305	10.260
ϵ(He–H)	5.761	6.325	4.239
σ(He–C_{methyl})[b]	⋯	⋯	3.239
σ(He–$C_{9,10}$)[c]	⋯	⋯	2.808

[a]References 45 and 46.
[b]Parameters for the two methyl group carbon atoms.
[c]$C_{9,10}$ denotes the two carbon atoms which are common to both aromatic rings of 2,3-DMN.

of 0.1 or 0.01 Å, and the well depths ϵ from 3.8 to 16.6 cm^{-1} in steps of 0.5 cm^{-1}. Further constraints on the parameter optimization were:

(i) The vibrationally averaged z (He-ring) distance to be $3.2\ \text{Å} < \langle z \rangle < 3.35\ \text{Å}$, since this is the range experimentally found for similar vdW complexes such as *s*-tetrazine·He,[1] benzene·He,[2] and *t*-stilbene.[16]

(ii) The calculated dissociation energy value to be within the experimentally determined limits of 2,3-DMN·He, established as $25.9\ cm^{-1} < D_0 < 163\ cm^{-1}$.[35]

Despite a very extensive search in LJ parameter space, employing a total of 400 separate DVR calculations, no parameter combinations were found with smaller RMS deviation between observed and calculated vdW vibrational frequencies than the starting $tHe-3$ parametrization. As an example, in Table I we give a parameter set, denoted I: the resulting calculated intermolecular vibrational frequencies, shown in Table II, differ by $>2\ cm^{-1}$ from experiment, similar to those obtained with $tHe-3$.

Much better agreement with the experiment was achieved by introducing additional flexibility into the parametrization: in analogy to our DVR calculations on 2,3-DMN·Ne,[32] we allowed the σ(He–C) parameter of the C_9 and C_{10} atoms (the C atoms common to the two rings) to vary, and found an optimum value of 2.808 Å. Additional improvement was found when changing the σ(He–C) parameter of the C atoms of the two methyl groups, by a factor of 1.045 relative to the I parametrization. This modified parameter set is denoted II, also given in Table I. This parameter set II is currently being employed for 3D DVR calculations of other aromatic molecule-helium complexes, such as *o*-xylene·He and toluene·He (published elsewhere), and yields good agreement with the experimental van der Waals vibrational frequencies.

TABLE II. Comparison of experimental and theoretical vdW frequencies (in cm^{-1}) of 2,3-DMN·He in the S_1 state, calculated with the three parameter sets *tHe*3, I and II given in Table I. Cartesian vibrational quantum number assignments are also given.

Experiment	*tHe*3[a]	Set I	Set II	(v_x, v_y, v_z)
5.0	⋯	⋯	⋯	isomer
10.3	8.66	8.33	10.34	(1,0,0)
18.4	16.97	16.19	18.19	(2,0,0)
22.7	24.67	24.13	22.98	(0,2,0)
25.9	26.79	25.50	25.70	(3,0,0)
RMS deviation	1.53	1.66	0.20	

[a]References 45 and 46.

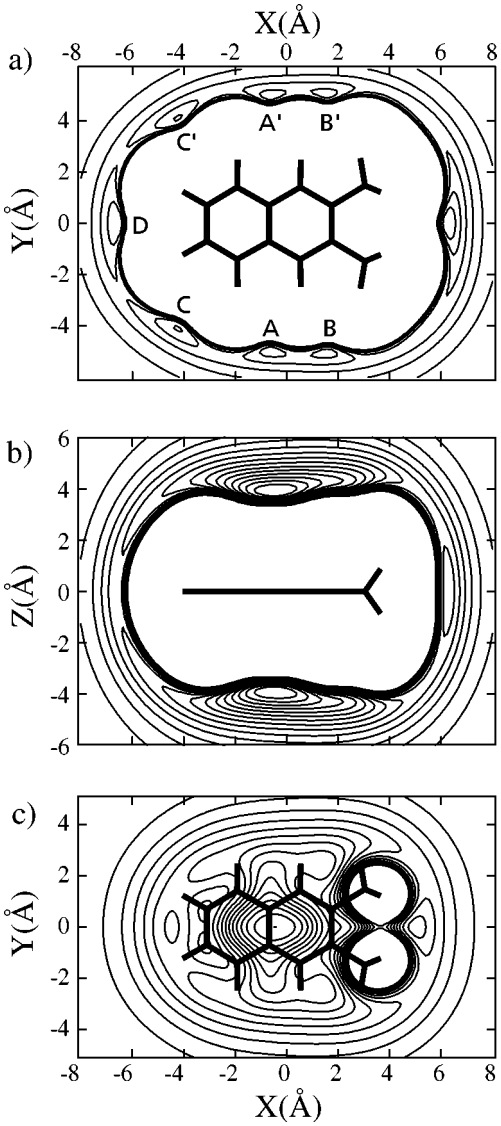

FIG. 2. Contour plots of the IPES of S_1 2,3-DMN·He for the LJ-parameter set II of Table I. Potential cuts in the xy plane, for $z = 0.0$ Å (a), xz plane for $y = 0.0$ Å (b) and xy plane for $z = 2.93$ Å (c) are shown. The first contour is drawn at 0.1 cm^{-1} above the global potential minimum located at $(x,y,z) = (-0.426, 0.0, \pm 2.93\ \text{Å})$. The energy spacing between subsequent contours is 7 cm^{-1}.

The IPES for S_1 2,3-DMN·He, using set II, is represented in Fig. 2, and is seen to be highly anharmonic in all three directions. The global potential minimum [Fig. 2(c)] is located over the C_9–C_{10} central bond of the napthalene moiety, in distinct contrast to the 2,3-DMN·Ne[32] and 2,3-DMN·Ar[25] complexes, for which the global minima are situated above the ring carrying the methyl groups. As Fig. 2(b) shows, there exist two symmetrically equivalent global minima, situated on either side of the molecular plane. These

TABLE III. Characteristic energy values (in cm^{-1}) of 2,3-DMN·He in the S_1 state, calculated with both the potential parameter sets I and II given in Table I.

	$D_{e,g}$	$D_{e,s}$	D_0	ZPE
Set I	−141.86	⋯	−90.15	51.71
Set II	−106.14	−48.47	−60.27	45.87

lie at $(x,y,z)_{gl}=(-0.426,0.0,\pm 2.93$ Å), with a calculated well depth $D_{e,g}=-106.15\ cm^{-1}$.

Figures 2(a) and 2(b) show the existence of a secondary minimum for 2,3-DMN·He, in which the He atom lies on the x axis, between the two methyl groups, at $(x,y,z)_s=(6.261,0.0,0.0$ Å), giving C_{2v} point group symmetry. The well depth is less than half that of the global minimum, being $D_{e,s}=-48.47\ cm^{-1}$. This local minimum is very shallow, lying merely $10\ cm^{-1}$ below the two symmetrically equivalent barriers E_{g-s}, E'_{g-s}, which connect it to the two global minima. These barriers lie between the methyl groups at $(x,y,z)_{g-s}=(5.516,0.0,\pm 2.543$ Å), at $67.10\ cm^{-1}$ above the global minimum. An analogous potential minimum was found for the 2,3-DMN·Ne complex, and gives rise to a second, experimentally detectable isomer.

There are no further minima in the intermolecular PES. However, Fig. 2(a) displays seven more stationary points lying in the xy plane: three pairs of saddle points denoted A/A', at $67.40\ cm^{-1}$, B/B', at $68.08\ cm^{-1}$, C/C', at $70.35\ cm^{-1}$, which occur at $\pm$ the same y value, all relative to the global minimum. A fourth saddle point D, which lies at $71.25\ cm^{-1}$, is unique. All seven saddle points have Hessian index one, and negative curvature along the z direction. They connect the two global minima along four distinct side-crossing paths; three of these occur in symmetry-equivalent pairs (''narcissistic'' pathways), while the path via D is unique. All four paths are *direct*, while a fifth side-crossing path leads indirectly from one global minimum via the secondary minimum to the other global minimum.

As will be seen below, the extent of delocalization of the He wave functions over the PES, as well as the tunneling splittings between symmetry-equivalent pairs of vibrational states, are influenced by the number and height of the side-crossing barriers, as well as the associated path lengths. It is important to investigate a numerically soluble case in which there is such a diversity of classical reaction pathways and barrier heights, and calculate the corresponding quantum mechanical probability densities.

B. Vibrational eigenvalues: theory and experiment

Table II compares the experimentally observed intermolecular vibrational transition frequencies of S_1 2,3-DMN·He with the 3D DVR vibrational frequencies calculated for sets $tHe-3$, I and II. Also given are the quantum number assignments (v_x,v_y,v_z) in terms of the number of quanta in the approximate Cartesian modes along the x, y, and z axes, which were made by inspection of the wave function plots. Table III lists the respective zero-point energies and D_0 values.

As Table II shows, all three parameter sets allow an assignment of the bands at at 10.3, 18.4, and $25.9\ cm^{-1}$ as a vibrational progression in the long-axis mode (v_x, 0,0) with $v_x=1-3$. However, only parametrization II is of acceptable accuracy, reproducing the level positions to within $\approx 0.2\ cm^{-1}$. The y-mode level (0,1,0) transforms as b_2, and is not symmetry-allowed as a fundamental. However, the first y overtone (0,2,0), calculated at $23.0\ cm^{-1}$ is observed as a weak band at $22.7\ cm^{-1}$.

The transition at $+5.0\ cm^{-1}$ could *not* be fitted in terms of a vdW vibrational excitation by *any* parametrization within the constraints mentioned in the previous section. Furthermore, parameter sets that *did* yield such a low-frequency excitation failed to reproduce the higher excitations, as well as yielding unacceptably low dissociation energies. We conclude that this band is *not* a vdW vibrational excitation, and postulate that it is due to the vdW isomer of C_{2v} geometry, with the He atom in plane and adjacent to the two methyl groups. As will be shown below, localized vdW vibrational states exist in the secondary minimum.

We note that the analogous 2,3-DMN·Ne complex also exhibits a band which is blue-shifted relative to the origin by $+5.0\ cm^{-1}$; in that case, the isomer hypothesis was supported by hole-burning experiments.[32] In the present case, the very low concentration of the complex in the molecular beam (about 1% of the 2,3-DMN signal), combined with the very low intensity of the $+5\ cm^{-1}$ band relative to the main electronic origin of 2,3-DMN·He, precluded an experimental verification of this hypothesis.

C. van der Waals vibrational states of S_1 2,3-DMN·He

According to the DVR calculations, the IPES with parametrization II supports 173 vdW vibrational states up to the dissociation limit. These states are qualitatively characterized by a set of wave function parameters:

(i) The expectation values of the Cartesian coordinates $\langle x\rangle$ and $\langle z\rangle$, which describe the vibrationally averaged geometry. Notice that $\langle y\rangle=0$ by symmetry. In principle, $\langle z\rangle=0$ also; however, in order to characterize the z location of the wave function relative to the molecular plane, we define $\langle z\rangle$ over the *positive* z range only.

(ii) The root-mean-square (RMS) amplitudes of the vdW vibrations, Δx, Δy, and Δz, along each of the Cartesian axes; these parameters measure the floppiness of the complex in its vibrational states. These are summarized in Tables IV–V for each IR in C_{2v}.

For about 90 vibrational wave functions, 3D wave function isosurfaces were generated, which reveal a fascinating diversity: out of the 173 states, 42 states (i.e., $13a_1$, $13b_1$, $8b_2$, and $8a_2$) can be considered as localized in the global minima. These lower-lying states all occur in pairs which are symmetric/antisymmetric with respect to the molecular plane (i.e., a_1/b_1 or a_2/b_2), and are nearly degenerate, with tunneling splittings $<0.1\ cm^{-1}$, cf. Tables IV–V. Three levels are localized in the C_{2v} local minimum, corresponding to ground and excited vibrational states of a vdW isomer; these do not occur in pairs. The other 128 vdW vibrational states

TABLE IV. Properties of the lowest 26 a_1 van der Waals vibrational levels of 2,3-DMN·He, calculated with the 3D DVR method, employing LJ parameter set II (Table I) ΔE_g in cm^{-1}, $\langle x\rangle$, $\langle z\rangle$, Δx, Δy, and Δz in Å. Cartesian quantum number assignments are given as (v_x, v_y, v_z).

n	ΔE_g	$\langle x\rangle$	$\langle z\rangle$	Δx	Δy	Δz	(v_x, v_y, v_z)
1	0.000	−0.357	3.222	0.655	0.582	0.315	(0,0,0)
2	10.336	0.068	3.318	1.225	0.631	0.333	(1,0,0)
3	18.190	0.250	3.381	1.664	0.708	0.357	(2,0,0)
4	22.977	−0.170	3.300	0.846	1.852	0.376	(0,2,0)
5	25.699	−0.062	3.426	2.045	0.776	0.379	(3,0,0)
6	29.792	0.574	3.333	1.373	2.044	0.401	(1,2,0)
7	32.314	−0.402	3.442	2.397	1.213	0.434	(4,0,0)
8	33.656	−0.152	3.088	1.132	2.791	0.541	(0,4,0)
9	37.122	−0.225	3.373	2.180	1.933	0.447	(2,2,0)
10	37.646	−0.549	3.390	2.611	1.810	0.526	(5,0,0)
11	39.092	0.065	3.179	1.982	2.646	0.733	(3,2,0)
12	39.700	−0.314	3.509	1.268	2.079	0.764	(0,0,1)
13	41.693	−0.578	3.262	3.384	1.892	0.760	(6,0,0)
14	42.058	−0.260	2.415	1.874	3.815	1.113	(0,6,0)
15	42.509	6.453	0.937	1.493	0.903	0.790	(0,0,0*)[a]
16	42.794	−1.050	3.220	2.784	2.359	0.670	(4,2,0)
17	44.831	−0.588	2.892	3.237	2.887	0.974	(5,2,0) ?[b]
18	44.947	−0.893	3.050	3.568	2.358	0.889	(7,0,0)
19	45.617	0.189	2.374	2.802	3.724	1.187	?[b]
20	46.492	−0.788	2.069	2.476	3.988	1.312	(0,8,0)
21	47.057	0.790	3.413	3.012	2.069	1.085	(1,0,1)
22	47.437	−1.495	2.604	4.312	2.229	1.302	(8,0,0) ?[b]
23	47.793	−1.079	2.320	2.696	3.686	1.228	?[b]
24	48.252	−1.232	2.639	3.459	3.139	1.194	?[b]
25	49.120	0.498	2.491	5.183	1.789	1.290	(9,0,0) ?[b]
26	49.315	1.331	2.055	4.507	3.501	1.232	?[b]

[a]Level localized in the secondary C_{2v} minimum.
[b]?: Assignment uncertain or impossible.

TABLE V. Properties of the 20 lowest b_2 van der Waals vibrational levels of 2,3-DMN·He, calculated using LJ parameter set II (Table I). Definitions and units as in Table IV.

n	ΔE_g	$\langle x\rangle$	$\langle z\rangle$	Δx	Δy	Δz	(v_x, v_y, v_z)
1	14.629	−0.281	3.302	0.726	1.224	0.334	(0,1,0)
2	22.837	0.392	3.389	1.281	1.369	0.354	(1,1,0)
3	28.673	−0.146	3.212	1.064	2.373	0.421	(0,3,0)
4	30.602	−0.072	3.381	1.653	1.636	0.395	(2,1,0)
5	34.555	0.273	3.204	1.637	2.584	0.470	(1,3,0)
6	37.165	−0.432	3.386	2.213	1.863	0.475	(3,1,0)
7	38.226	−0.071	2.811	1.089	3.400	0.710	(0,5,0)
8	40.737	−0.723	3.243	2.440	2.456	0.580	(4,1,0)
9	42.567	0.132	2.744	2.110	3.487	0.836	(2,3,0)
10	43.536	−0.462	2.789	2.214	3.259	1.066	[0,5,0]
11	44.210	−0.655	2.299	2.037	3.933	1.204	?[b]
12	45.071	−0.665	2.775	2.740	3.242	1.037	(4,3,0)
13	46.882	−1.225	2.422	3.270	3.515	1.273	?[b]
14	47.817	−0.300	3.087	3.301	2.807	0.818	(5,1,0)
15	47.953	0.780	1.995	2.618	4.263	1.233	(0,9,0)
16	48.642	−0.578	2.703	2.831	3.228	1.510	(0,1,1)
17	48.945	4.696	1.568	3.185	2.901	1.244	(0,1,0*)[a]
18	49.585	−0.565	2.530	3.451	3.339	1.315	?[b]
19	49.997	−0.053	2.634	3.476	3.253	1.337	?[b]
20	50.713	0.469	2.395	2.471	3.865	1.417	(0,3,1)

[a]Level localized in the secondary C_{2v} minimum.
[b]?: Assignment uncertainties or impossible.

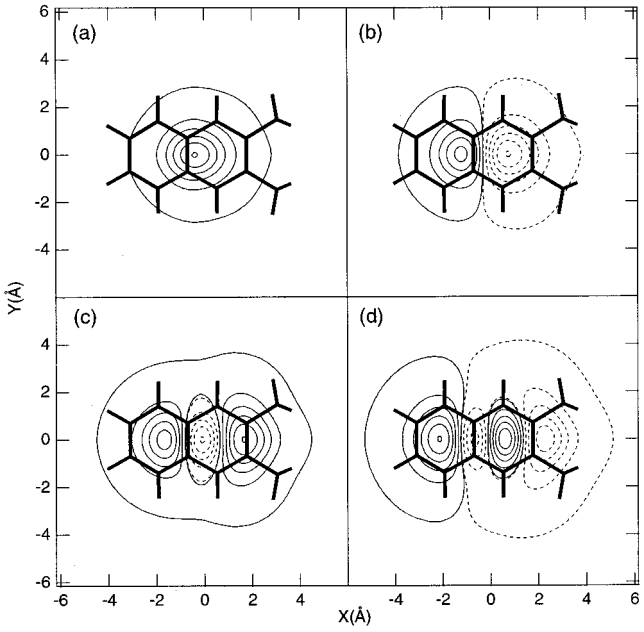

FIG. 3. The xy-plane cuts through wave functions (0,0,0), (1,0,0), (2,0,0) and (3,0,0) localized in the global minimum. Contours are at 99, 90, 80, 60, 40, 20, and 1% of the maximum amplitude for the respective cuts. Solid (dashed) curves enclose regions of positive (negative) amplitude.

can be considered delocalized over the entire surface of the 2,3-DMN aromatic molecule. For delocalized states, corresponding symmetric/antisymmetric level pairs can be identified up to a vibrational energy of $\approx 50\ \mathrm{cm}^{-1}$, or $10\ \mathrm{cm}^{-1}$ below the dissociation limit. These pairs of states show increasingly large tunneling splittings, growing from $\approx 0.1\ \mathrm{cm}^{-1}$ to $>3\ \mathrm{cm}^{-1}$. These three classes of vdW vibrational states are now presented separately, followed by a discussion of the tunneling splittings.

1. van der Waals states associated with the global minimum

For these levels, the wave functions are roughly centered above the molecule at $x=0.0\pm 0.4$ Å, and at $z=\pm 3.3$ ± 0.15 Å from the molecular plane. Typically, states of all irreps up to energies $\Delta E_g = 42\ \mathrm{cm}^{-1}$ belong to this category. We first examine the states corresponding to pure x-axis or y-axis excitations. Cuts of typical wave functions belonging to this category are shown in Fig. 3. They include the vibrational ground state (0,0,0), as well as the states assigned as (1,0,0), (2,0,0), and (3,0,0), which were experimentally observed. The node(s) along the x axis can be seen clearly.

Such states were identifiable by their nodal structure up to 9 or 10 quanta in x, and up to 9 quanta in y, cf. Tables IV and V. Fig. 4 shows the associated RMS amplitudes, Δx and Δy. Up to $v_x=5$, $v_y=6$, the RMS amplitudes increase smoothly and almost linearly with vibrational quantum number. Starting with $v_x=6$, $v_y=7$, the RMS vibrational amplitudes show strong deviations from a linear increase, in some cases even *decreasing* with increasing quantum number. This is due to: (i) the finite size of the substrate molecule, which sets a limit to the growth of the spatial extent of the

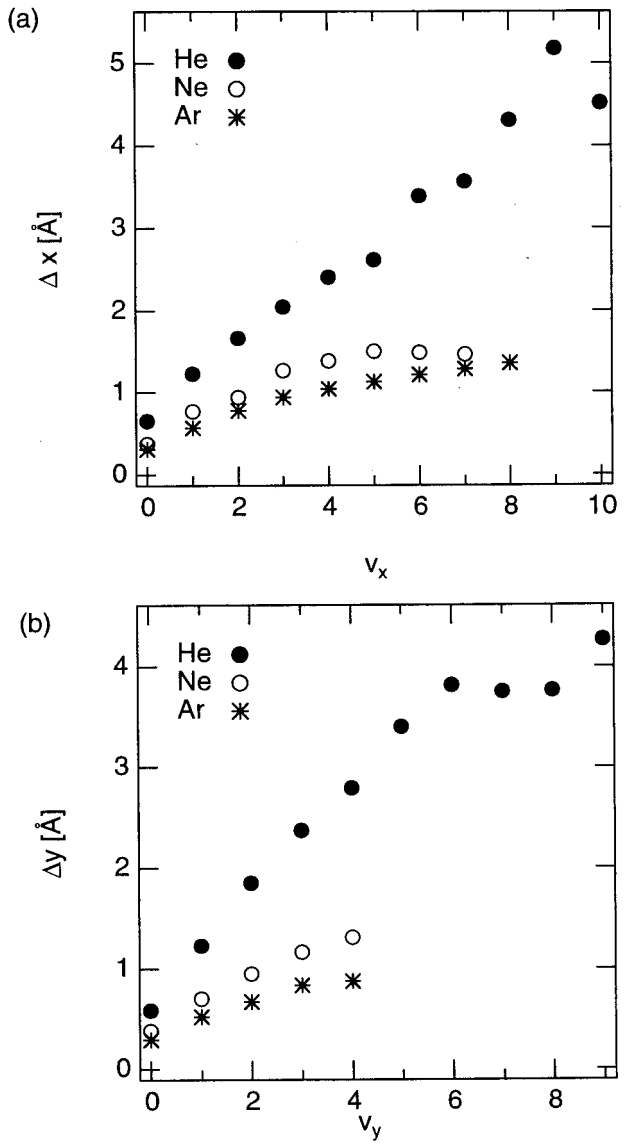

FIG. 4. Root-mean-square amplitudes (in Å) (a) Δx for states $(v_x,0,0)$ as a function of v_x, and (b) Δy for states $(0,v_y,0)$ as a function of v_y, shown for 2,3-DMN·He (●), 2,3-DMN·Ne (○), and 2,3-DMN·Ar (∗).

wave function, as measured by Δx, Δy; (ii) the onset of extensive side-crossing delocalization of the wave functions (see also below), leading to strong coupling of the x and y motion with the z degree of freedom, so that a decrease in Δx and/or Δy may be compensated by an increase in Δz; (iii) the onset of extensive anharmonic couplings between states of the same irrep, due to the rapid increase in level density, which ultimately leads to a breakdown of the classification of states as ''pure'' x, y, or z states.

Many states with simultaneous excitation in x and y can also be identified and assigned Cartesian quantum numbers. However, some states can be classified more clearly in terms of a 2D isotropic oscillator, with radial quantum number n, and angular quantum number l, labelled by brackets as $[n,l,v_z]$. An example is listed in Table V, the [0,5,0] angular oscillator state $n=10(a_2)$ and $10(b_2)$.

Interestingly, although the global minimum supports

about 40 levels with varying degrees of excitation *parallel* to the molecular plane, only a single pair of excitations was found corresponding to a purely *perpendicular* or z-mode excitation. This is the pair of states $12(a_1)/12(b_1)$. Table IV shows that these states are characterized by an especially large value $\langle z\rangle = 3.51$ Å. No other vibrational states were found up to the dissociation limit with such a large $\langle z\rangle$ value, and extensive examination of wave functions up to high energies did not disclose any states with two nodes in the z direction. We conclude that only a *single pure z* excitation is stable in this intermolecular potential.

2. van der Waals states localized in the secondary C_{2v} minimum

There are only three vdW states localized at the secondary C_{2v} minimum of the IPES: these are the local ground state $n=15$ (a_1), the local z fundamental $n=19$ (b_1), and the local y fundamental $n=17$ (b_2). Isosurfaces of these three states are shown in Fig. 5. There does not seem to be a local x fundamental supported by this local potential minimum, as judged by the calculated $\langle x\rangle$ and Δx values. This lack of stability of vdW excitations directed radially outwards from the aromatic molecule qualitatively agrees with the finding of the previous section on the lack of higher z excitations associated with the global minimum.

3. Delocalized and side-crossing van der Waals vibrational states

We characterize the extent of side-crossing delocalization by the magnitude of the wave functions at the side-crossing barriers A, A', B, B',.... For the wave functions of IR's a_2 and b_1, the amplitudes are zero due to the existence of a mirror plane. For the wave functions of a_1 and b_2 IR's, we classify a state as delocalized if its magnitude in the $z=0$ plane is $>30\%$ of the maximum amplitude. This amplitude criterion roughly corresponds to an energy criterion, namely a calculated tunneling splitting of 0.1 cm^{-1} (see below).

Using the amplitude criterion, side-crossing delocalization occurs at a well-defined energy onset, starting with $n=14$ at $\Delta E_g = 42.058$ cm^{-1} for the a_1 states (see Fig. 6), and with $n=9$ at $\Delta E_g = 42.567$ cm^{-1} for the b_2 states, see Fig. 7. This energy of $\Delta E_g \approx 42$ cm^{-1} corresponds to about 70% of D_0. At higher energies, delocalized states are the rule, occasionally interspersed with localized states. The side-crossing states are characterized not only by large values of Δx and/or Δy, but also a large Δz, in combination with a low $\langle z\rangle$, indicating that amplitude has moved from above and below the molecular plane to the peripheral regions around the aromatic molecule.

Although all the side-crossing barriers A, B, C, D of the IPES are quite close in energy, the wave functions tend to concentrate at a single barrier (or single pair of side-crossing barriers). Thus, the a_1 wave functions $n=14$ (see Fig. 6), 18, 20, and 23 are all concentrated at the pair of barriers A,A'. The $n=17$ wave function (see Fig. 8) concentrates at C,C', $n=19$ at B,B', and $n=21$ at the single barrier D. For the

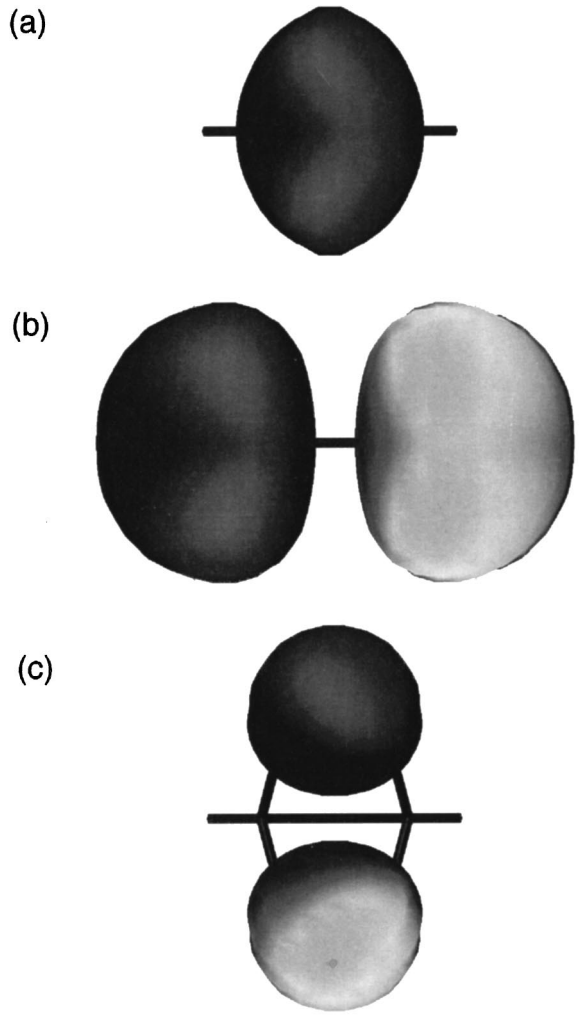

FIG. 5. The 3D isosurfaces of the wave functions of the three vdW states localized at the secondary C_{2v} minimum. Isosurfaces are drawn at 30% of the maximum amplitude, dark (light) surfaces enclose regions of positive (negative) amplitude: (a) the local vibrationless state, (b) the local y fundamental, (c) the local z fundamental (see text).

FIG. 6. The 3D isosurface (at 56% amplitude level) of the lowest vdW vibrational state (14, a_1) at 42.058 cm^{-1} which exhibits sizable (larger than 0.3) amplitude at a side-crossing barrier. Wave-function delocalization occurs at the side-crossing lowest barriers A, A' [see Fig. 2(a)].

FIG. 7. The 3D isosurface (at the 30% amplitude level) of the lowest vdW vibrational state (9, b_2) at 42.567 cm^{-1} which delocalizes via the barriers B, B', see Fig. 2(a).

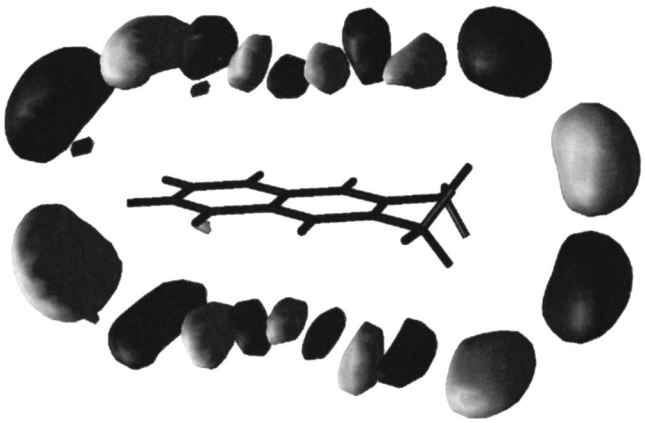

FIG. 9. The 3D isosurface of the lowest vdW vibrational state (22, a_1) at 47.437 cm^{-1}, which exhibits complete delocalization around the host molecule in the xz plane.

delocalized b_2 wave functions, $n=9$ crosses at the barriers B,B' (Fig. 7), and $n=13$ crosses dominantly at the C,C' barriers. With increasing energy, wave functions begin to spread over two close-lying barriers. Thus the b_2 wave functions $n=10$ and 11 cross at both the B,B' and A,A' barriers, $n=13$ crosses dominantly at the C,C' barriers, while $n=19$ crosses at the A,A' and C,C' barriers.

The state (22, a_1) at 47.44 cm^{-1} shown in Fig. 9 is the first to display complete delocalization around the 2,3-DMN molecule, in the xz plane. This wave function may also be viewed as a *high-l internal rotation* state, with the He atom rotating completely around the aromatic molecule (note that all calculations here are for zero *total* angular momentum). The analogous $J>0$ states will ultimately become metastable with respect to dissociation at some J value. Such quasibound states are *orbiting resonances*,[7] which play an important role for collisional rotational energy transfer from or to the aromatic molecule, and were postulated as important metastable intermediates in the formation of vdW complex in the rapidly cooling translational bath of the supersonic expansion.[7]

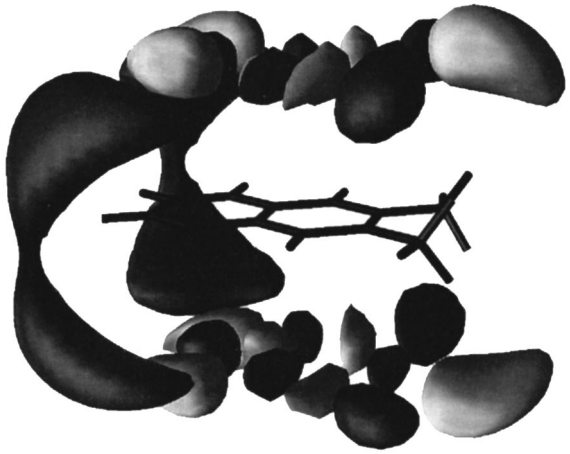

FIG. 8. The 3D isosurface (at the 27% amplitude level) of the lowest vdW vibrational state (17, a_1) at 44.831 cm^{-1} which delocalizes via the barriers C, C', see Fig. 2.

4. van der Waals mode dependence of tunneling splittings

A different diagnostic criterion of side-crossing delocalization is the size of the calculated tunneling splittings between the a_1/b_1 (or a_2/b_2) members of the tunneling pair. These were extracted from Tables IV and V, and are given in Table VI. For the lowest vdW states, the tunneling splitting is $\ll 0.0001$ cm^{-1}, below the numerical precision of the computational procedure. Beginning at ≈ 30 cm^{-1}, the splittings increase to >0.001 cm^{-1}.

In the energy range from 30 to 50 cm^{-1}, corresponding members of tunneling pairs can be clearly identified from their wave function shapes and nodal structures. The largest tunneling splitting between an *identifiable* pair of levels is for the y-mode (0,8,0) pair, being 3.2 cm^{-1}. The corresponding isosurfaces are shown in Fig. 10.

The logarithm of the tunneling splitting shows an approximately linear dependence on total intermolecular vibrational energy, as is seen in Fig. 11(a). In the limit of strong mixing of the intermolecular degrees of freedom, one expects that the tunneling rates become independent of the specific mode, depending only on some effective 1D tunneling coordinate, and the total intermolecular energy. For a 1D parabolic barrier to side-crossing, the semiclassical WKB approximation predicts that tunneling splittings should have an exponential dependence on total intermolecular energy, as is indeed found.

Closer examination of Fig. 11(a) reveals deviations from this exponential energy dependence, which are due to *mode-specific* tunneling rates. Examining the tunneling splittings for the series of pure x-mode and pure y-mode excitations, one observes that the y-mode tunneling splittings are always larger than the x-mode splittings at the same *energy*, as shown in Fig. 11(a), and also for equal *quantum number*, see Fig. 11(b), although the barriers are of almost equal height.

TABLE VI. Calculated tunneling splittings Δ (in cm^{-1}) between the (a_1/b_1) and (a_2/b_2) pairs for splittings $>10^{-3}\,cm^{-1}$. Assignments in terms of cartesian quantum numbers (v_x,v_y,v_z) are also given. The states are sorted by increasing energy ΔE_g.

a_1	b_1	Δ	(v_x,v_y,v_z)
8	8	0.005	(0,4,0)
9	9	0.001	(2,2,0)
10	10	0.002	(5,0,0)
11	11	0.037	(3,2,0)
12	12	0.012	(0,0,1)
13	13	0.033	(6,0,0)
14	14	0.524	(0,6,0)
16	15	0.063	(4,2,0)
17	16	0.090	(5,2,0)
18	17	0.098	(7,0,0)
19	18	0.490	?[a]
20	24	3.282	(0,8,0)
21	20	0.276	(1,0,1)
22	22	1.099	(8,0,0)
23	21	0.204	?[a]
24	23	0.599	?[a]
a_2	b_2	Δ	(v_x,v_y,v_z)
5	5	0.002	(1,3,0)
6	6	0.003	(3,1,0)
7	7	0.074	(0,5,0)
8	8	0.017	(4,1,0)
9	9	0.144	(2,3,0)
10	10	0.224	[0,5,0]
12	11	0.091	(4,3,0)

[a]Assignment uncertain or impossible.

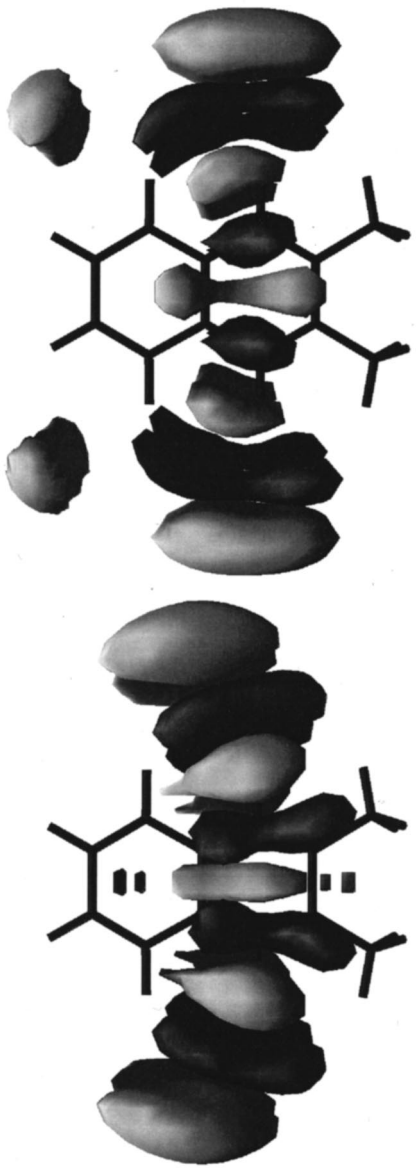

FIG. 10. The 3D isosurfaces of the wave functions of the two vdW (0,8,0) states (20, a_1), (24, b_1) which comprise the tunneling pair with the largest tunneling splitting of 3.28 cm^{-1} (see Table VI). Isosurfaces are drawn at 40% of the maximum level.

This is due to (i) the shorter side-crossing path length along the yz direction, compared to the xy direction, combined with (ii) the smaller moment of inertia of the 2,3-DMN substrate for counter-rotation around the y axis, which governs the effective mass for side-crossing motion in the yz-plane. Hence the splitting rises more rapidly with v_y than with v_x. However, for each mode taken individually, the tunneling splitting increases exponentially with energy, as the effective 1D model predicts [see Fig. 11(a)].

For increasing intermolecular vibrational energy, it becomes increasingly difficult to identify corresponding pairs of symmetric/antisymmetric levels, due to the high level density, and the onset of extensive anharmonic mode mixing. In some cases, the near resonant state mixings give rise to apparent *negative* tunneling splittings, i.e., cases where the antisymmetric level is seemingly lower in energy than its symmetric counterpart. This seeming violation of a basic quantum mechanical principle only reflects the fact that in a coupled multimode system, an additional nodal plane along one direction can be energetically compensated by subtle wave function changes along other coordinates.

By comparing the energies of the lowest-energy levels that are considered to be delocalized across a certain type of barrier, i.e., A, B, C, or D, the vibrationally adiabatic barriers can be determined. As discussed earlier for 2,3-DMN·Ne[32] and the prototypical isomerizing molecule HCN/HNC,[43] these effective, dynamical barriers control the onset of wave function delocalization between two (or more) potential minima. Thus (14, a_1), which is the first state to side-cross at A,A', lies at $-18.22\,cm^{-1}$, while the potential barrier lies at $-38.75\,cm^{-1}$; thus the intermolecular ZPE at this barrier is $20.53\,cm^{-1}$. This is considerably lower than the intermolecular ZPE at the global minimum, which is $45.9\,cm^{-1}$ (see Table III). In other words, while the side-crossing barrier of the IPES has a height of $67.4\,cm^{-1}$ above the potential minimum, the vibrationally adiabatic barrier decreases to only $42.06\,cm^{-1}$ above the vibrationless level.

Similarly, for the first state to delocalize across the single barrier pair C,C', the potential barrier is $70.35\,cm^{-1}$, while the vibrationally adiabatic barrier is $44.83\,cm^{-1}$. Finally, for the first state to delocalize across the single barrier D, which is (21, a_1), the vibrationally adiabatic barrier is

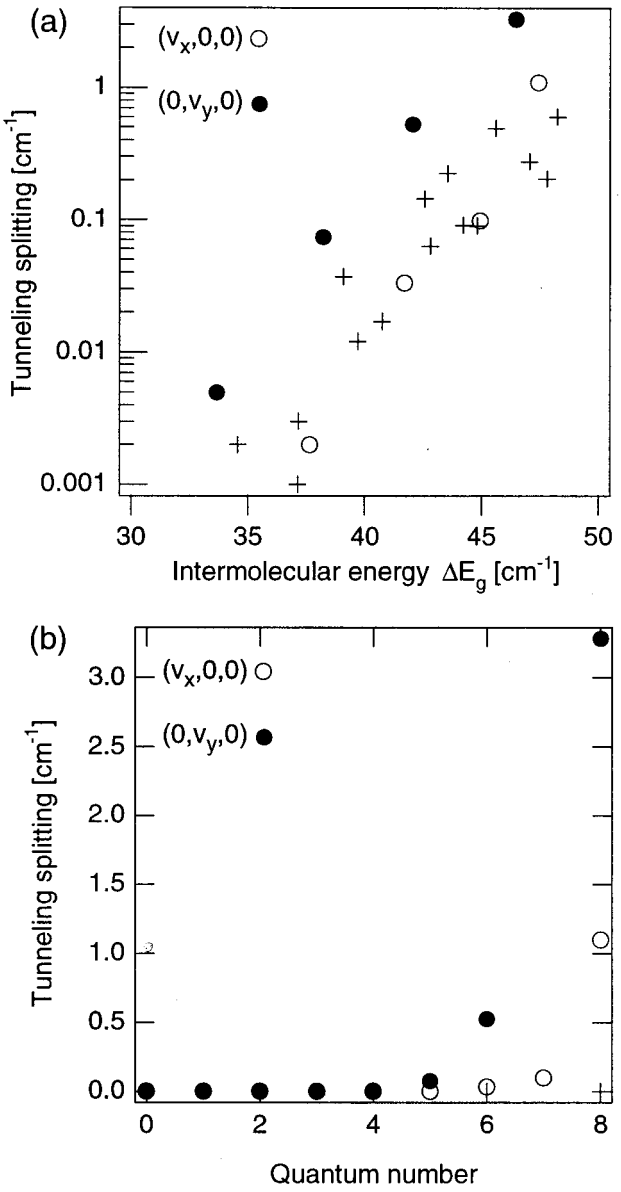

FIG. 11. (a) Tunneling frequency splitting between all pairs of intermolecular vibrational states vs intermolecular energy in the 30–50 cm^{-1} range, showing a roughly exponential increase with energy; (b) Frequency splitting for tunneling pairs of pure x and y excitations vs quantum number v_x or v_y.

47.44 cm^{-1}, while the potential barrier is 71.25 cm^{-1}. In all cases, the effective barrier decrease is $\approx$24–25 cm^{-1}.

V. COMPARISON OF THEORETICAL RESULTS FOR THE COMPLEXES OF He, Ne, AND Ar WITH 2,3-DMN

The present study of the intermolecular vibrations of 2,3-DMN·He complements our earlier combined experimental and theoretical investigations of related vdW complexes 2,3-DMN·Ar[25] and 2,3-DMN·Ne,[32] all in the S_1 electronic state. In this section, we compare the salient features of the intermolecular potential energy surfaces (IPESs) and the quantum dynamics of vdW vibrations of these three complexes, for the S_1 electronic state.

TABLE VII. Characteristic energies (in cm^{-1}) of the calculated S_1 state intermolecular PES's of 2,3-DMN·R complexes with R=He, Ne, Ar: well depths of the global minima ($D_{e,g}$), of the local (secondary) C_{2v} minima ($D_{e,s}$), barrier heights to side crossing ($E_{sc,A}$) and to isomerization between the global and secondary minima (E_{g-s}), and zero-point energies of the intermolecular vibrations (ZPE).

R	$D_{e,g}$	$D_{e,s}$	$E_{sc,A}$[a]	E_{g-s}[a]	ZPE
He	−106.2	−48.5	67.4	67.1	45.9
Ne[b]	−211.2	−99.0	127.1	146.4	32.0
Ar[c]	−429.6	−165.9	285.3	316.2	35.1

[a]Relative to the global minimum ($D_{e,g}$) of the respective vdW complex.
[b]From Ref. 25.
[c]From Ref. 32.

The IPESs of 2,3-DMN·R (R=He,Ne,Ar) complexes are strongly anharmonic and have three potential minima, which are qualitatively similar to those shown in Fig. 2 for 2,3-DMN·He. Two of them are symmetrically equivalent global minima located above and below the aromatic ring plane of 2,3-DMN. The third minimum, considerably shallower than the global minima, has a C_{2v} geometry corresponding to the rare-gas atom on the x axis and in the plane of 2,3-DMN, between the two methyl groups. Two distinct isomers (vdW conformers) associated with the global minimum (dominant isomer) and the local C_{2v} minimum (minor isomer), respectively, have been observed for 2,3-DMN·Ne[32] and 2,3-DMN·He.

The theoretical values for the well depths of the global and local (secondary) minimum, $D_{e,g}$ and $D_{e,s}$ respectively, as well as the minimum-energy barriers for side crossing at the saddle points A,A' ($E_{sc,A}$), and for isomerization between the global and secondary minimum, E_{g-s}, are given in Table VII. It must be pointed out that these values should be taken as semiquantitative at best. For all three vdW complexes, the Lennard-Jones (LJ) parameters which define the pairwise additive IPESs have been fit to a small number (4–7) of low-energy bands attributed to intermolecular vibrations of the dominant, minimum-energy isomer of 2,3-DMN·R (R=He,Ne,Ar). The available experimental data are only weakly sensitive to $D_{e,g}$ and provide no constraints on the higher-energy regions of the IPES close to the side-crossing and isomerization barriers, or in the vicinity of the secondary C_{2v} minimum. With this caveat in mind, we note that the global-minimum well depths $D_{e,g}$ of the He, Ne, and Ar complexes with 2,3-DMN exhibit an approximate ratio 1:2:4. Interestingly, the potential barrier heights $E_{sc,A}$ and E_{g-s} of the three vdW dimers display roughly the same relationship.

Despite the large differences in $D_{e,g}$'s and rare-gas atom masses ranging from 4 to 40 amu, the fundamental vdW frequencies of 2,3-DMN·R (R=He,Ne,Ar) dimers listed in Table VIII show a surprisingly weak dependence on the identity of the rare-gas atom. The quantities which display much larger variation from one 2,3-DMN·R complex to another are the RMS amplitudes of the intermolecular vibrations, in particular Δx and Δy for the in-plane x and y modes. Figure 4 shows Δx and Δy of the progressions in the

TABLE VIII. Fundamental frequencies (in cm^{-1}) of the intermolecular x, y, and z modes for 2,3-DMN·R complexes with R=He, Ne, Ar from quantum 3D calculations. The results for Ne and Ar complexes are from Refs. 32 and 25, respectively.

R	ν_x	ν_y	ν_z
He	10.3	14.6	39.7
Ne[a]	8.4	12.2	37.2
Ar[b]	8.3	16.8	41.6

[a]From Ref. 32.
[b]From Ref. 25.

x mode $(v_x,0,0)$ and y mode $(0,v_y,0)$, for 2,3-DMN·R (R=He,Ne,Ar). It is evident that for equal $v_x(v_y)$, $\Delta x(\Delta y)$ is much larger in 2,3-DMN·He than in 2,3-DMN·Ne and 2,3-DMN·Ar. This is expected in view of the fact the He atom is five times lighter than the Ne atom, and ten times lighter than Ar. In fact, the ratios of the RMS amplitudes $\Delta x(\mathrm{He})/\Delta x(\mathrm{Ne})$ and $\Delta x(\mathrm{He})/\Delta x(\mathrm{Ar})$ are reasonably well reproduced by a simple harmonic oscillator model; the same is true for the Δy's. Moreover, $\Delta x(\mathrm{He})$ and $\Delta y(\mathrm{He})$ grow much more rapidly with increasing v_x and v_y, respectively, than the same RMS amplitudes in the other two vdW complexes. Clearly, the floppiness of 2,3-DMN·He along the x and y coordinates exceeds by far that of 2,3-DMN·Ne and 2,3-DMN·Ar. This holds for Δz as well, which is 0.315 Å in the ground vdW state of the He complex, compared to 0.11 and 0.16 Å for the ground states of the corresponding Ar and Ne complexes, respectively.[25,32]

Another important feature varies widely among the 2,3-DMN·R (R=He,Ne,Ar) complexes studied by us is the energy threshold for wave function delocalization over two or all three minima on the IPES. Table VII shows large differences in the minimum-energy barriers to side crossing ($E_{sc,A}$) and isomerization between the global and local C_{2v} minimum (E_{g-s}) for the three vdW dimers. Based on Table VII, classical thresholds for delocalization (by side crossing) lie at 67, 127, and 285 cm^{-1}, for the complexes of He, Ne, and Ar with 2,3-DMN, respectively, measured from the global minimum $D_{e,g}$ of the respective dimer. This classical picture is in accord with our quantum 3D calculations, which for 2,3-DMN·He have revealed that the first vdW level showing significant side crossing is at 87.9 cm^{-1} (level $n=14$ of a_1 symmetry in Table IV), while the first level delocalized over the global *and* local C_{2v} minima lies at 93.3 cm^{-1} (level $n=22$ of a_1 symmetry in Table IV), both measured from the global minimum. In 2,3-DMN·Ne,[32] the first state extensively delocalized over all three minima lies at 162.4 cm^{-1} relative to the global minimum; as expected, this is considerably higher than the quantum delocalization threshold(s) in 2,3-DMN·He.

In the case of 2,3-DMN·Ar, our 3D DVR calculations produced converged vdW levels up to ~ 100 cm^{-1} relative to the global minimum,[25] well below the barriers $E_{sc,A}$ and E_{g-s} of 285.3 and 316.2 cm^{-1}, respectively. It would be prohibitively costly in terms of computer time and memory to extend these calculations to excitation energies in excess of 300 cm^{-1} (from the global minimum), necessary to determine the onset of delocalization in this system.

VI. CONCLUSIONS

The intermolecular vibrations and van der Waals isomerism of 2,3-dimethylnaphthalene·He were studied both theoretically and experimentally. This system exhibits prototypical features of three-dimensional large-amplitude vibrational motion hitherto unexplored in aromatic molecule/ rare-gas complexes. Two-color resonant two-photon ionization spectra of the $S_0 \rightarrow S_1$ electronic transition of this complex exhibit five bands within 30 cm^{-1} to the blue of the electronic origin.

The IPES was modeled as a pairwise sum of atom–atom Lennard-Jones potentials; it exhibits two symmetry-equivalent global minima on each side of the naphthalene moiety, and a single shallower local minimum adjacent to the two methyl groups. There are ten distinct saddle points connecting these three minima.

Accurate three-dimensional quantum calculations of the van der Waals vibrational levels were performed, using the 3D DVR method. Beginning with the $tHe3$ parametrization of Lim,[45,46] we studied a large range of four-parameter LJ sets. Within the experimental constraints imposed by reproducing both known He–aromatic molecule bond distances and dissociation energies of this and analogous He vdW complexes,[10–16,35,36] no parameter set reproduced the observed vibrational levels to <1.5 cm^{-1} RMS deviation. By introducing two additional LJ parameters for the methyl group C atoms and the central C atoms of the naphthalene ring, the four observed vibrational bands could be reproduced with an RMS deviation of <0.2 cm^{-1}.

Three observed vdW vibrational excitations could be assigned as a progression in the long-axis in-plane x mode with $v_x=1-3$, and the fourth band as an overtone of the short-axis y mode. The fundamental vdW frequencies predicted by this IPES are $\nu_x=10.3$ cm^{-1}, $\nu_y=14.6$ cm^{-1}, and $\nu_z=39.7$ cm^{-1}. The predicted vibrationally averaged distance of the He atom from the naphthalene aromatic plane is $\langle z_0 \rangle = 3.22$ Å. The predicted binding energy of the He atom is $D_0(S_1)=60.3$ cm^{-1}. All values agree with or are compatible with experiments.

The fifth observed band was assigned as the electronic origin of the van der Waals isomer corresponding to the local minimum of the IPES. The isomer vibrational ground state is calculated to lie 42.5 cm^{-1} above the global ground state. The local minimum supports only two local vdW vibrational excitations, both oriented tangential to the 2,3-DMN molecule, with calculated frequencies $\nu_z=4.2$ cm^{-1} and $\nu_y=6.4$ cm^{-1}.

The DVR calculations give 173 bound vdW vibrational states up to the dissociation limit for the IPES with the final parameter set. The lowest 42 states are localized, i.e., associated with the two global minima. The highest of these lie at ≈ 41 cm^{-1}, equivalent to $\approx 65\%$ of $D_0(S_1)$. However, even the vibrational ground state exhibits a large in-plane (x/y) RMS wavefunction amplitude of 0.7 Å.

Most low-lying vdW vibrational states occur in pairs which are symmetric/antisymmetric with respect to the naphthalene molecular (xy) plane. For these pairs the wavefunction delocalization around the molecule leads to ''side-crossing'' tunneling splittings. From the vibrational ground state up to 30 cm^{-1} vibrational energy, the calculated splittings are $\ll 0.0001$ cm^{-1}, which is only resolvable by microwave or high-resolution cw laser spectroscopy. The in-plane RMS amplitudes grow almost linearly with increasing v_x or v_y up to ≈ 5 Å. The associated tunneling splittings increase to ≈ 0.1 cm^{-1} at 42 cm^{-1}, and to >3 cm^{-1} at 48 cm^{-1}, which should be resolvable with pulsed dye lasers. Beyond ≈ 50 cm^{-1} the symmetric/antisymmetric pairs of states can no longer be unequivocally identified, due to strong anharmonic coupling with other vdW states of the same symmetry.

Overall, the tunneling splittings increase roughly exponentially with intermolecular vibrational energy, as expected for tunneling through an effective one-dimensional parabolic barrier. More-detailed examination reveals strong mode specificity of the tunneling splittings: at any given energy, pairs of states extending along the short in-plane y axis typically have three to ten times larger tunneling splittings than those along the long in-plane or x axis. The mode specificity is due to (i) the shorter side-crossing path length along the y direction, (ii) the existence of six barriers along the y direction, compared to only two barriers along the x direction, (iii) the smaller moment of inertia of 2,3-DMN molecule for the side-crossing motion in the y than in the x direction. Although there are eight distinct side-crossing saddle points on the IPES which lie quite close in energy, the lower-lying delocalized wave functions cross the molecular plane at only one barrier (or symmetry-equivalent pair of barriers).

The IPES parameters developed and optimized in this work are currently being applied to the calculation of structural and vibrational properties of similar aromatic molecule–helium complexes, such as toluene·He, xylene·He, and 1,8-DMN·He.[36] The forthcoming vibrational levels results are in excellent agreement with experiments, indicating that the potential parameters developed here are transferable and may be generally applicable for such He vdW complexes and clusters.

ACKNOWLEDGMENTS

A.B. and S.L. thank the Schweiz. Nationalfonds for support (Project Nos. 20-40669.94 and 20-487.96), and the Swiss Center for Superconducting (SCSC) at Manno for generous grants of computer time. Z.B. and D.S. gratefully acknowledge support from the National Science Foundation Grant CHE-9613641.

[1] R. E. Smalley, L. Wharton, D. H. Levy, and D. W. Chandler, J. Chem. Phys. **68**, 2487 (1978).
[2] S. M. Beck, M. G. Liverman, D. L. Montsand, and R. E. Smalley, J. Chem. Phys. **70**, 232 (1979).
[3] D. H. Levy, C. A. Haynam, and D. V. Brumbaugh, Faraday Discuss. Chem. Soc. **73**, 137 (1982).
[4] T. S. Zwier, M. Carrasquillo, and D. H. Levy, J. Chem. Phys. **78**, 5493 (1983).
[5] J. Hager and S. C. Wallace, J. Phys. Chem. **87**, 2121 (1983).
[6] A. Haynam, D. V. Brumbaugh, and D. H. Levy, J. Chem. Phys. **80**, 2256 (1984).
[7] T. Stephenson and S. A. Rice, J. Chem. Phys. **81**, 1083 (1984).
[8] E. R. Bernstein, K. Law, and M. Schauer, J. Chem. Phys. **80**, 207 (1984).
[9] E. R. Bernstein, K. Law, and M. Schauer, J. Chem. Phys. **80**, 634 (1984).
[10] C. A. Taatjes, W. B. Bosma, and T. S. Zwier, Chem. Phys. Lett. **128**, 127 (1986).
[11] D. H. Semmes, J. S. Baskin, and A. H. Zewail, J. Am. Chem. Soc. **109**, 4104 (1987).
[12] K. Yamanouchi, S. Isogai, and S. Tsuchiya, Chem. Phys. **116**, 123 (1987).
[13] D. O. DeHaan, A. L. Holton, and T. S. Zwier, J. Chem. Phys. **90**, 3952 (1989).
[14] T. S. Zwier, J. Chem. Phys. **90**, 3967 (1989).
[15] D. H. Semmes, J. S. Baskin, and A. H. Zewail, J. Chem. Phys. **92**, 3359 (1990).
[16] J. S. Baskin and A. H. Zewail, J. Chem. Phys. **93**, 5701 (1989).
[17] L. Yu, J. Williamson, S. C. Foster, and T. A. Miller, J. Chem. Phys. **97**, 5273 (1992).
[18] T. Brupbacher and A. Bauder, Chem. Phys. Lett. **173**, 435 (1990).
[19] T. Brupbacher, J. Makarewicz, and A. Bauder, J. Chem. Phys. **101**, 9736 (1994).
[20] A. Bauder, in *Molecular Dynamics and Jet Spectroscopy*, edited by J. M. Hollas and D. Phillips (Blackie Academic, London, 1993), p. 765.
[21] T. Weber, A. v. Bargen, E. Riedle, and H. J. Neusser, J. Chem. Phys. **92**, 90 (1990).
[22] T. Weber, E. Riedle, H. J. Neusser, and E. W. Schlag, J. Mol. Spectrosc. **249**, 69 (1991).
[23] T. Weber, E. Riedle, H. J. Neusser, and E. W. Schlag, Chem. Phys. Lett. **183**, 77 (1991).
[24] E. Riedle, R. Sussman, Th. Weber, and H. J. Neusser, J. Chem. Phys. **104**, 865 (1996).
[25] M. Mandziuk, Z. Bačić, T. Droz, and S. Leutwyler, J. Chem. Phys. **100**, 52 (1994).
[26] T. Droz, S. Leutwyler, M. Mandziuk, and Z. Bačić, J. Chem. Phys. **101**, 6412 (1994).
[27] T. Droz, S. Leutwyler, M. Mandziuk, and Z. Bačić, J. Chem. Phys. **102**, 4715 (1995).
[28] P. Parneix, N. Halberstadt, Ph. Bréchignac, F. G. Amar, A. van der Avoird, and J. W. I. van Bladel, J. Chem. Phys. **98**, 2709 (1993).
[29] J. Faeder, J. Chem. Phys. **99**, 7664 (1993).
[30] A. van der Avoird, J. Chem. Phys. **98**, 5327 (1993).
[31] E. Riedle and A. van der Avoird, J. Chem. Phys. **104**, 882 (1996).
[32] T. Droz, S. Leutwyler, M. Mandziuk, and Z. Bačić, J. Chem. Phys. **103**, 4855 (1995).
[33] B. Coutant and P. Brechignac, J. Chem. Phys. **100**, 7087 (1994).
[34] M. Mandziuk and Z. Bačić, J. Chem. Phys. **98**, 7165 (1993).
[35] A. Bach, T. Droz, and S. Leutwyler, to be submitted to J. Chem. Phys.
[36] A. Bach, S. Leutwyler, and Z. Bačić (in preparation).
[37] X.-Q. Tan, D. J. Clouthier, R. H. Judge, D. F. Plusquellic, and D. W. Pratt, J. Chem. Phys. **95**, 7862 (1991).
[38] M. Mandziuk and Z. Bačić, J. Chem. Phys. **101**, 2126 (1994).
[39] G. Brocks and D. van Koeven, Mol. Phys. **63**, 999 (1988).
[40] Z. Bačić and J. C. Light, Annu. Rev. Phys. Chem. **40**, 469 (1989).
[41] Z. Bačić, in *Domain-Based Parallelism and Problem Decomposition Methods in Computational Science and Engineering*, edited by D. E. Keyes, Y. Saad and D. G. Truhlar (SIAM, Philadelphia, 1995), p. 263.
[42] Z. Bačić and J. C. Light, J. Chem. Phys. **85**, 4594 (1986).
[43] Z. Bačić and J. C. Light, J. Chem. Phys. **86**, 3065 (1987).
[44] D. T. Colbert and W. H. Miller, J. Chem. Phys. **96**, 1982 (1992).
[45] K. F. Lim, J. Chem. Phys. **100**, 7385 (1994).
[46] K. F. Lim, J. Chem. Phys. **101**, 8756 (1994).